

# Compact Stars in the vBag Model and Its $f$ -Mode Oscillations

Heng-Yi Zhou <sup>1,2,†</sup> , Wei Wei <sup>3,†</sup>  and Xia Zhou <sup>1,4,5,\*</sup> 

<sup>1</sup> Xinjiang Astronomical Observatory, Chinese Academy of Sciences, Urumqi 830011, China; zhouhengyi@xao.ac.cn

<sup>2</sup> University of Chinese Academy of Sciences, 19A Yuquan Road, Beijing 100049, China

<sup>3</sup> College of Science, Huazhong Agricultural University, Wuhan 430079, China; weiwei1981@mail.hzau.edu.cn

<sup>4</sup> Key Laboratory of Radio Astronomy, Chinese Academy of Sciences, Nanjing 210008, China

<sup>5</sup> Xinjiang Key Laboratory of Radio Astrophysics, Urumqi 830011, China

\* Correspondence: zhouxia@xao.ac.cn

† These authors contributed equally to this work.

**Abstract:** Electromagnetic (EM) observations and gravitational wave (GW) measurements enable us to determine the mass and radius of neutron stars (NSs) and their tidal deformability, respectively. These parameters offer valuable insights into the properties of dense matter in NSs. In this study, the vector-interaction-enhanced bag model (vBag model) is employed to investigate strange and hybrid stars' properties. The parameters of the vBag model are constrained using multi-messenger observations, revealing that strange stars are incompatible with current observations. In contrast, hybrid stars can exhibit a substantial mixed phase region and a thin hadronic shell. Furthermore, we present the frequencies and damping time of fundamental mode ( $f$ -mode) oscillations of hybrid stars and test their universal relations with compactness and tidal deformability. The findings indicate that the presence of mixed phase components leads to larger frequencies and shorter damping time of the  $f$ -mode oscillation of hybrid stars, and the softer equation of state (EoS) affects this behavior more significantly. The universal relations of hybrid stars in the vBag model can be described by fourth-order/seventh-order polynomials, which do not break the previous results.

**Keywords:** equation of state; quark matter; compact stars



**Citation:** Zhou, H.-Y.; Wei, W.; Zhou, X. Compact Stars in the vBag Model and Its  $f$ -Mode Oscillations. *Universe* **2023**, *9*, 285. <https://doi.org/10.3390/universe9060285>

Academic Editors: Ana Gabriela Grunfeld and David Blaschke

Received: 5 May 2023

Revised: 1 June 2023

Accepted: 7 June 2023

Published: 10 June 2023



**Copyright:** © 2023 by the authors. Licensee MDPI, Basel, Switzerland. This article is an open access article distributed under the terms and conditions of the Creative Commons Attribution (CC BY) license (<https://creativecommons.org/licenses/by/4.0/>).

## 1. Introduction

The study of the structure of compact stars depends on the understanding of the EoS of the dense matter in them. It was conjectured a long time ago that quark matter appears inside compact stars, as strange stars or hybrid stars [1–3]. Recently, the Advanced LIGO and Advanced Virgo collaborations observed the binary neutron star (BNS) merger event GW170817 [4], which focused on the constraints on the compact stars' EoSs [5–9]. It appears possible, but not conclusive, that one or both component stars in the merger could be stars with quark matter [10–12]. Some examples of massive pulsars are observed ( $M > 2 M_{\odot}$ ) [13–16], combined with mass and radius measurements taken by the NICER (Neutron star Interior Composition Explorer) experiment [17–20], have provided, until recently, the most important benchmarks for the EoS. However, it has been pointed out that most of the current EoSs describing quark matter are too soft to support strange stars with large masses and are thus unable to explain the existence of massive pulsars [21,22].

The MIT bag model is a phenomenological approach to describe a confined system of relativistic quarks and gluon fields [23]. Calculations using soft EoSs of quark matter, such as the MIT bag model, provide values of maximum masses for strange stars lower than  $1.6 M_{\odot}$ . In this scenario, strange stars seem to be incompatible with the observed massive pulsars mentioned above. However, many studies found that effects from strong interactions, such as one-gluon exchange or color superconductivity, can stiffen the quark matter EoS [24,25]. Calculations of strange stars using the modified MIT bag model

(such as thermodynamic bag model (tdBag model) [26], non-ideal bag model [27], and vector MIT bag model [28,29]) or the Nambu–Jona–Lasinio (NJL) model [30,31] are capable of reproducing a maximum star mass of around  $2 M_{\odot}$ , which is compatible with the observational data [32,33].

Among these modified MIT bag models, a recent specific model inspired by non-perturbative features of quantum chromodynamics (QCD), namely, the vector-interaction-enhanced bag model (vBag model) [28], indicates that massive compact stars with mass  $\geq 2 M_{\odot}$  would be interpreted as possible candidates for strange stars. The vBag model was first introduced by Klähn and Fischer [28] and provides a stiff EoS, which is a hybrid approach to consolidate a number of seeming discrepancies between the NJL and tdBag model and is compatible with some of those observational data. However, the reasonable parameter range of this model is not clearly known. Motivated by these investigations, the first aim of this work is to fully and systematically exploit the constraints on the vBag model caused by the stable existence of strange quark matter and the multi-messenger observations.

Mapping out the radial or nonradial oscillation mode, including the fundamental ( $f$ ) mode, pressure ( $p$ ) mode, and gravity ( $g$ ) mode, can provide a way to probe the internal structure and composition of compact stars [34–39]. These modes are also known as quasinormal modes in relativistic fluid stars, and the oscillations of the stars are dissipated by gravitational radiation [40–42]. Among these modes, the  $f$ -mode is important for compact stars since its frequency,  $\sim 1$ – $3$  kHz, makes it relatively easier to be observed than other modes. On the other hand,  $f$ -mode oscillations can be excited in a wide range of astrophysical environments that are an effective source of gravitational radiation [40,42]: core-collapse supernova explosions, starquakes associated with a pulsar glitch, a binary compact star merger remnant [41]. Therefore, this makes the  $f$ -mode more likely to be detected by third-generation gravitational wave detectors, such as the Einstein Telescope (ET) [43] and the Cosmic Explorer (CE) [44] and future observation runs by LIGO, Virgo, and KAGRA [45].

Although the macrostructure of compact stars is sensitive to EoSs, insensitive relations connect various quantities of compact stars [40,46–50]. These relations are considered universal since they are highly insensitive to EoSs. In astrophysics and fundamental physics, universal relations for compact stars are essential. These relationships allow us to extract the macrostructure of compact stars with greater accuracy and assist in studying the inverse problem of identifying the EoS by giving EoS-insensitive linkages between distinct quantities. The second aim of the work is to test the universal relations between the frequency and damping time of the quadrupolar  $f$ -mode and the compactness and tidal deformability of hybrid stars using EoS parameter constraints from multi-messenger observations.

Previous works have constrained the bag constant of the MIT bag model and suggested possible values for hybrid stars by combining data from 20 compact star candidates [51]. Anisotropic compact star models also have been compared with the results of six compact star candidates [52]. The EoS models can be further constrained by the new observational data, especially the measurement of neutron star radii by the NICER mission. In this work, the vBag model is used to describe quark matter, and the mixed phase is constructed with the Gibbs construction. We constrain the parameter space of the vBag model within the strange stars and hybrid stars using current multi-messenger observations. Based on the parameter space constraints, we present the properties of  $f$ -mode oscillations of the hybrid star and improve the universal relations between  $f$ -mode frequency and the macrostructure of hybrid stars. The paper is organized as follows. Section 2 introduces the EoS and the macrostructure of the strange stars and hybrid stars used in this study. The results of multi-messenger constraints on the EoS parameters of quark matter are given in Section 3. In Section 4, we study the properties of  $f$ -mode and the universal relations of hybrid stars in the vBag model. Section 5 summarizes the main points of this work.

## 2. EoS and Macrostructure of Compact Stars

In this work, the relativistic Dirac–Brueckner–Hartree–Fock approach (DBHF) is used to describe the hadronic matter [53], which can account for the properties of many-body nuclear matter and is compatible with astronomical observations. For quark matter, it is described by the vBag model. The mixed phase is constructed using Gibbs construction [54]. For the crust, we use the simple BBP and BPS models to describe the inner and outer structures [55,56], which are widely used models that consider the interaction of the electron gas with the nuclei, as well as the effect of the dripped neutrons, and can describe the properties of matter in the low-density region of a neutron star. Due to uncertainties with different crust models, one may obtain slightly different mass-radius relations.

### 2.1. Hadronic Phase

When modeling the behavior of cold hadronic matter for astrophysical applications, an excellent approximation for the specific energy of neutron-rich matter has been revealed by many studies [38,53]:

$$E(n, x) = E\left(n, x = \frac{1}{2}\right) + S(n)(1 - 2x)^2, \tag{1}$$

where  $x$  is the proton fraction,  $E\left(n, x = \frac{1}{2}\right)$  is the energy per particle of symmetric nuclear matter, and  $S(n)$  is the nuclear symmetry energy. Then, by applying simple thermodynamic relations to an ensemble describing matter that adheres to the conditions of  $\beta$ -equilibrium and charge neutrality, we obtain the nuclear pressure and energy density.

The model we adopt is a general method used to describe the energy of nucleons in the hadronic phase, where the energy per particle of symmetric nuclear matter and the nuclear symmetry energy is obtained using the DBHF model [57,58]. This model’s calculations meet the empirical saturation point of nuclear matter with a binding energy of  $-16$  MeV at the saturation density [57]. Furthermore, at the saturation density, the DBHF model provides a symmetry energy of 35 MeV, which is in good agreement with the empirical models and data from isospin diffusion in heavy-ion collisions. The derivative of the symmetry energy with respect to number density is 69.4 MeV, which is also called symmetry pressure and indicates that nuclear matter is relatively soft at saturation density [59]. In addition, the DBHF model produces a neutron star with a maximum mass of  $2.3 M_{\odot}$ . Thus, in an analysis of the DBHF model and its performance under a neutron star and heavy-ion collision constraints, this particular EoS performs extremely well (see Fuchs [57], Klähn et al. [59] for further references).

### 2.2. Quark Phase

We use the vBag model to describe the quark matter. The pressure and energy density of a single flavor can be expressed as [28]:

$$P_f(\mu_f) = P_{FG,f}(\mu_f^*) + \frac{K_v}{2} n_{FG,f}^2(\mu_f^*) - B_{\chi,f}, \tag{2}$$

$$\epsilon_f(\mu_f) = \epsilon_{FG,f}(\mu_f^*) + \frac{K_v}{2} n_{FG,f}^2(\mu_f^*) + B_{\chi,f}, \tag{3}$$

where  $P_{FG,f}(\mu_f^*)$  and  $\epsilon_{FG,f}(\mu_f^*)$  are the pressure and energy given by a Fermi gas expression of the individual flavor quark. The second term, which contains  $K_v$ , is from the vector interaction. The effective flavor chemical potential  $\mu_f^*$  is determined self-consistently at a given bare flavor chemical potential

$$\mu_f = \mu_f^* + K_v n_{FG,f}(\mu_f^*). \tag{4}$$

The number density is

$$n_f(\mu_f) = n_{FG,f}(\mu_f^*), \tag{5}$$

and  $B_{\chi,f}$  is the bag constant of a single flavor. The introduction of flavor-dependent chiral bag constants is motivated by their fits to the pressure of the chirally restored phase, and a deconfinement bag constant  $B_{dc}$  is introduced to lower the energy/particle and thereby favor stable strange matter. Thus, the EoS of the vBag model can be written as [28]

$$P_q = \frac{1}{3} \left( \epsilon_q - 4 \sum_f B_{\chi,f} \right) + \frac{4}{3} B_{dc} + \frac{K_v}{3} \sum_f n_f^2(\mu_f), \tag{6}$$

where the free parameters are vector interaction coupling constant  $K_v$  and effective bag constant  $B_{eff} = \sum_f B_{\chi,f} - B_{dc}$ .

### 2.3. Mixed Phase: Gibbs Construction

The dense matter in the compact star satisfies  $\beta$ -equilibrium, which relates to the chemical potentials in nuclear and quark matter at low temperatures. Together with the charge neutrality conditions in each phase, it is evident that one chemical potential is sufficient to characterize the individual thermodynamic state of nuclear and quark matter if no phase transition is assumed. If both phases are independent, the phase with the higher pressure minimizes the thermodynamical potential and is therefore energetically favorable. Consequently, a phase transition will occur if nuclear and quark matter have equal pressure at the equal baryochemical potential [60],

$$P^H(\mu_B) = P^Q(\mu_B), \tag{7}$$

where  $P^H$  and  $P^Q$  are the pressures of the hadronic and quark phases, respectively.  $\mu_B$  is the baryon chemical potential. The baryon number and the total electric charge are conserved in the quark deconfinement phase transition. The phase transition between hadronic and quark phases occurs over a range of pressures and chemical potentials, where both phases coexist in a mixed phase region. Thus, the mixed phase is given by the condition [60], and the global charge neutrality condition satisfied by the Gibbs construction can be expressed as

$$(1 - \eta)Q^H + \eta Q^Q = 0, \tag{8}$$

where  $\eta = V^Q / (V^Q + V^H)$  is the volume fraction occupied by quark matter, and  $\eta$  ranges from 0 to 1. Thus, the total energy density of the mixed phase is

$$\epsilon = (1 - \eta)\epsilon^H + \eta\epsilon^Q. \tag{9}$$

### 2.4. Macroscopic Structure of Compact Stars

In order to obtain the mass ( $M$ ) and radius ( $R$ ) of non-rotating compact stars, we solve the Tolman–Oppenheimer–Volkoff (TOV) equations [60–62]:

$$\begin{aligned} \frac{dP}{dr} &= \frac{(P + \epsilon)(m + 4\pi r^3 P)}{r(r - m)}, \\ \frac{dm}{dr} &= 4\pi r^2 \epsilon. \end{aligned} \tag{10}$$

Tidal deformability is also one of the macroscopic properties of a compact star, which reflects the ability of a neutron star to deform under a tidal field. It is also the most important one carrying information about the EoS of compact stars. The dimensionless tidal deformability is defined as

$$\Lambda = \frac{2}{3} k_2 C^{-5}, \tag{11}$$

where  $C = M/R$  is the compactness of the star. By solving the differential equation of Love number  $k_2$  together with the TOV equations and the EoS, the dimensionless tidal deformability can be obtained [63–65].

The parameters  $K_V$  and  $B_{\text{eff}}$  play an important role in the properties of compact stars described in our work. We give out the mass–radius relations of strange stars and hybrid stars with different  $K_V$  and  $B_{\text{eff}}$  in Figures 1 and 2.  $K_V$  and  $B_{\text{eff}}$  decide the stiffness of the EoS of quark matter, which affects the maximum mass and radius of both strange stars and hybrid stars. For strange stars, the maximum mass and radius increase with the increase in  $K_V$  and decrease in  $B_{\text{eff}}$  because the larger the value of  $K_V$  is and the smaller the value of  $B_{\text{eff}}$  is, the stiffer the EoS of the quark matter is. For hybrid stars, the maximum mass is more sensitive to the value of  $K_V$  among two parameters: it increases with the increase in  $K_V$ . By choosing appropriate values of  $K_V$ , the maximum mass of the hybrid star can exceed  $2 M_\odot$ . Both  $K_V$  and  $B_{\text{eff}}$  affect the radii of hybrid stars obviously. The radius increases with the increase in  $K_V$  and  $B_{\text{eff}}$ . The critical masses for the appearance of quarks depend on  $K_V$  and  $B_{\text{eff}}$  too. The mixed phase appears earlier for smaller values of  $K_V$  or  $B_{\text{eff}}$ , and the critical mass is more sensitive to  $B_{\text{eff}}$ . With fixed  $K_V$ , the smaller  $B_{\text{eff}}$  is, the earlier the mixed phase appears, the smaller the critical mass is. For some parameter combinations, the mixed phase appears at a density even lower than nuclear saturation density, which indicates a large quark fraction might exist even in the low-mass stars. Moreover, the early phase transition leads to the increased compactness of stars and thus to smaller radii. For hybrid star models, the critical masses range from around  $0.2 M_\odot$  to near the maximum mass of DBHF EoS ( $2.3 M_\odot$ ), i.e. it is possible to obtain low mass and more compact hybrid stars for the Gibbs construction.

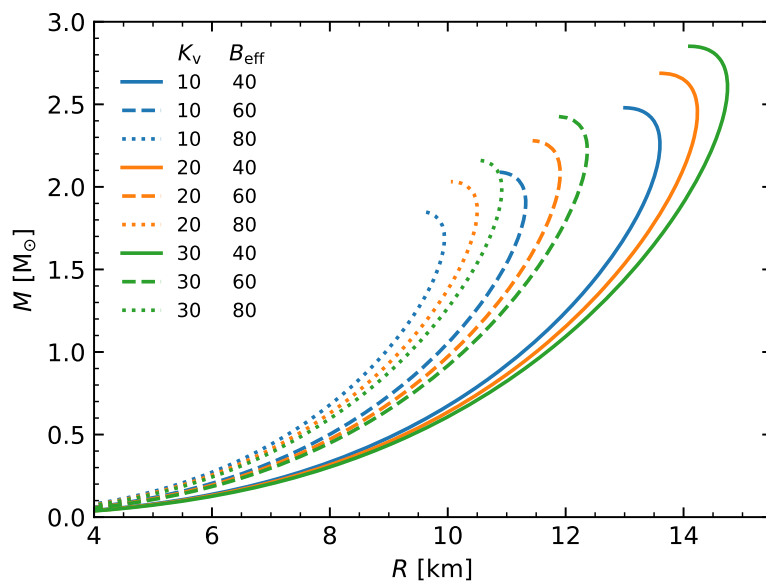


**Figure 1.** Mass–radius relations for strange stars in the vBag model. The blue, orange, and green lines are for  $K_V = 10, 20,$  and  $30 \text{ GeV}^{-2}$ , respectively. The solid, dashed, and dotted lines are for  $B_{\text{eff}} = 40, 60,$  and  $80 \text{ MeV fm}^{-3}$ , respectively.

Under the Gibbs construction, the densities of mixed phase vary from  $\sim 1$  to 10 nuclear saturation density, making it impossible for the central density of a stable hybrid star to reach the pure quark phase. In addition, no pure quark phase exists in the core of hybrid stars in the vBag model. Therefore, our results indicate that earlier phase transitions and a wide range of mixed phase densities make it only possible for quarks to be present in the mixed phase with the Gibbs construction of hybrid stars.

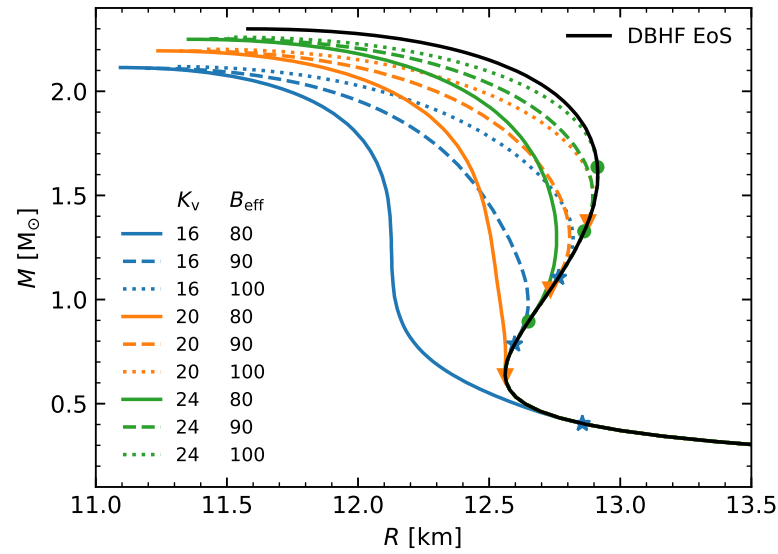


**Figure 2.** Mass–radius relations for hybrid stars in the vBag model. The solid black line shows the result for normal neutron stars with DBHF EoS. The blue, orange, and green lines are for  $K_V = 16, 20,$  and  $24 \text{ GeV}^{-2}$ , respectively. The solid, dashed, and dotted lines are for  $B_{\text{eff}} = 80, 90,$  and  $100 \text{ MeV fm}^{-3}$ , respectively. The stars, triangles, and dots on the DBHF EoS curve in this figure correspond to the masses and radii at which the mixed phases start to emerge inside the neutron stars with each  $K_V$ .

In Figure 3, we give the ratio of  $R_{\text{mp}}/R$  and  $M_{\text{mp}}/M$  ( $R_{\text{mp}}$  is the radius from the center of the star to the surface of the mixed phase,  $M_{\text{mp}}$  is the mass enclosed within  $R_{\text{mp}}$ ,  $R$  and  $M$  are the full radii and mass of the star). We find that the ratio of the radius and mass of the mixed phase increases with the total mass of the hybrid star. For massive stars, the mixed phase occupies a large fraction of the star, and the mixed phase mainly contributes to the mass of the hybrid star. The ratio of the radius and mass of mixed phase can even exceed 0.8 for some parameters, since these EoS are softer.

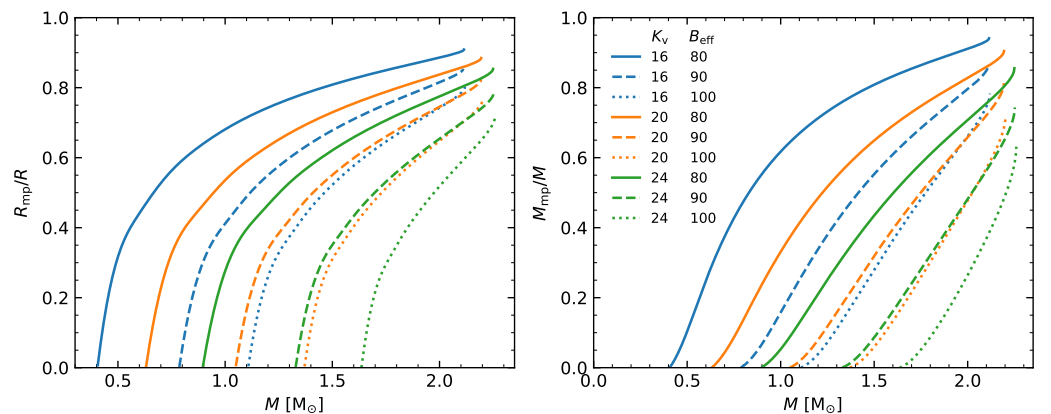


**Figure 3.** The correlations between  $R_{\text{mp}}/R$  (left panel) and  $M_{\text{mp}}/M$  (right panel) and the total mass  $M$  of the hybrid star. The color scheme is the same as in Figure 2.

### 3. Constraints on the EoS of Quark Matter in the vBag Model

The electromagnetic (EM) observations for the mass and radius of NSs require that the EoSs must be stiff enough to support the  $2 M_{\odot}$  star, and the GW measurements for tidal deformability require that the EoSs are not too stiff. Therefore, combining the results of EM and GW results in a good constraint for the EoSs of dense matter. In this work, we use the following multi-messenger (EM and GW) astrophysical observations:

- Massive pulsars. PSR J1614–2230 with  $M = 1.908^{+0.016}_{-0.016} M_{\odot}$  [13,66], PSR J0348+0432 with  $M = 2.01 \pm 0.04 M_{\odot}$  [14], and PSR J0740+6620 with  $M = 2.08 \pm 0.07 M_{\odot}$  [16]. PSR

J1810+1744 and PSR J0952–0607, with  $M = 2.13 \pm 0.04 M_{\odot}$  and  $M = 2.35 \pm 0.17 M_{\odot}$ , respectively [67,68]. According to the above massive pulsars observations, the maximum mass of the star must be higher than  $2 M_{\odot}$ .

- The radii of neutron stars’ constraints from NICER mission. PSR J0030+0451 with  $M = 1.34^{+0.15}_{-0.16} M_{\odot}$ ,  $R = 12.71^{+1.14}_{-1.19}$  km [17] and  $M = 1.44^{+0.15}_{-0.14} M_{\odot}$ ,  $R = 13.02^{+1.24}_{-1.06}$  km [19]. PSR J0740+6620 with  $M = 2.072^{+0.067}_{-0.066} M_{\odot}$ ,  $R = 12.39^{+1.30}_{-0.98}$  km [18] and  $M = 2.08 \pm 0.07 M_{\odot}$ ,  $R = 13.7^{+2.6}_{-1.5}$  km [20].
- Current bounds for the effective tidal deformability as reported by the LIGO–Virgo collaboration have been placed at  $\bar{\Lambda} = 300^{+420}_{-230}$  at a 90% confidence for low-spin priors [45]. Furthermore, the dimensionless tidal deformability of a star at the Chandrasekhar mass has been reported at  $\Lambda_{1.4} = 190^{+390}_{-120}$  under the same conditions [4,69].

By adopting the above observational results, we give out the parameter space of the vBag model ( $K_v$ ,  $B_{\text{eff}}$ ) within strange stars, and the results are shown in Figure 4. The stability window bounded by the “two-flavor line” (the energy per particle  $E/A = 934$  MeV) and “three-flavor line” ( $E/A = 930.4$  MeV) are also given out. The “2-flavor line” ensures the normal atomic nuclei will not decay into nonstrange quark matter (above the line), while the “3-flavor line” ensures strange quark matter will be more stable than normal nuclear matter (below the line) [70,71]. When all observational and stability limitations are addressed, no parameter space of the quark matter in the vBag model can simultaneously fulfill multi-messenger observations. This indicates that strange stars in the vBag model that correspond to present constraints may not exist.

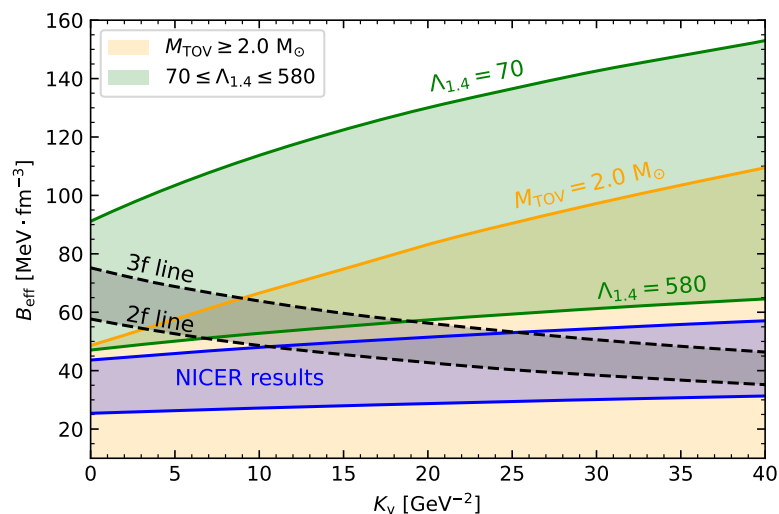


**Figure 4.** The parameter space of the vBag model ( $K_v$  and  $B_{\text{eff}}$ ) for a strange star. The orange contour represents the parameter space where the star’s maximum mass is greater than  $2 M_{\odot}$ . The green contour represents the parameter space for the tidal deformability  $70 \leq \Lambda_{1.4} \leq 580$  from the GW170817 event. The blue contour is for the parameter space that satisfies the mass and radius measurements of PSR J0030+0451 and PSR J0740+6620 from NICER. The black dashed lines are for the 2-flavor and 3-flavor lines of quark matter, and the gray contour is for the stability windows of quark matter.

The parameter space constraints of the vBag model within hybrid stars are shown in Figure 5. In the vBag model, the positive value of the bag constant  $B_{\text{eff}}$  results only from the restoration of chiral symmetry, while confinement/deconfinement, although introduced merely phenomenologically, reduces this value. The most naive perception of confinement is the binding of quarks in the chirally broken phase [28]. Therefore, the lower limit of  $B_{\text{eff}} \geq 70 \text{ MeV fm}^{-3}$  of the vBag model in the mixed phase with DBHF EoS is needed. The gray contour between the green and blue lines is the parameter space of the quark matter EoS in the hybrid star that satisfies the observational constraints. It is worth to

mention that Figure 5 only shows the limit of the tidal deformability  $\Lambda_{1.4} = 580$  from GW170817. With the current constraints,  $\Lambda_{1.4}$  of the hybrid star with the softest EoS is  $\sim 300$ . To achieve the best display effect, this figure does not show the lower limit  $\Lambda_{1.4} = 70$ . Due to the phase transition inside the compact star, the emergence of new particle degrees of freedom will soften the EoS, thereby making the star become denser, and finally satisfying the constraints of tidal deformability from GW170817. This reveals that the quark matter in the vBag model would exist in the core of the compact star.

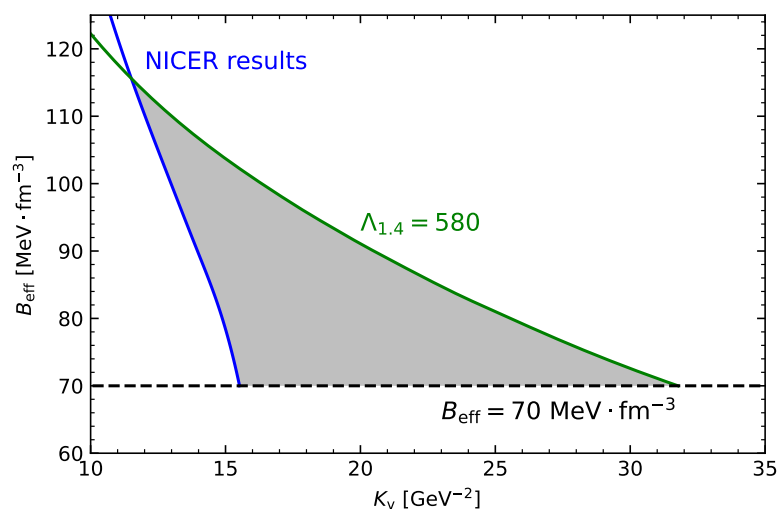


**Figure 5.** Constraints on  $K_v$  and  $B_{\text{eff}}$  of hybrid stars with Gibbs construction in the vBag model. The green line is for the constraint of the dimensionless tidal deformability  $\Lambda_{1.4} = 580$ . The blue line is for the EoS parameters boundary that satisfies the observational data of mass and radius of PSR J0030+0451 and PSR J0740+6620 from NICER. The dashed black line is the lower boundary  $B_{\text{eff}} = 70 \text{ MeV} \cdot \text{fm}^{-3}$ . The gray contour is the parameter space of quark matter EoS in the hybrid star that satisfies the observational constraints.

#### 4. The f-Mode Oscillations and Related Universal Relations of Hybrid Stars in the vBag Model

Since the parameter space of the vBag model satisfying the current observations in strange stars may not exist, we only investigate the quadruple fundamental mode ( $\ell = 2$  f-mode) oscillations of hybrid stars, which are constructed as the previous section. The method of solving the oscillation of hybrid stars is introduced in Lindblom and Detweiler [72], Detweiler and Lindblom [73]. A fully general relativistic approach is adopted in our work, which takes into account both fluid and spacetime perturbations and is more suitable for extreme general relativistic effects on compact stars.

In Figure 6, the f-mode frequency  $f_f$  and damping time  $\tau_f$  are shown as a function of the stellar mass for different EoS parameters of quark matter. We also give the corresponding results of a neutron star in a DBHF EoS for comparison. The frequency of the neutron star in the DBHF EoS is  $\sim 1.53\text{--}2.21$  kHz, and the damping time is  $\sim 0.147\text{--}0.455$  for  $M \geq 1.0 M_\odot$ . From this figure, one can see that these properties vary with  $K_v$  and  $B_{\text{eff}}$ . The appearance of quark matter inside the hybrid star will increase the frequency  $f_f$  and decrease the damping time  $\tau_f$  of the f-mode, respectively. Moreover, the increase in  $K_v$  leads to an increase in the f-mode frequency and a decrease in the damping time. With the same  $K_v$ ,  $B_{\text{eff}}$  affects the magnitude of the frequency and the damping time significantly, indicating the f-mode oscillation is very sensitive to the mass and radius of the star. We also find that the frequencies increase gradually with the mass of hybrid stars, but this behavior becomes steeper when the mass is close to  $M_{\text{max}}$ , and the damping time decreases rapidly with the mass of hybrid stars until it is close to  $M_{\text{max}}$ .

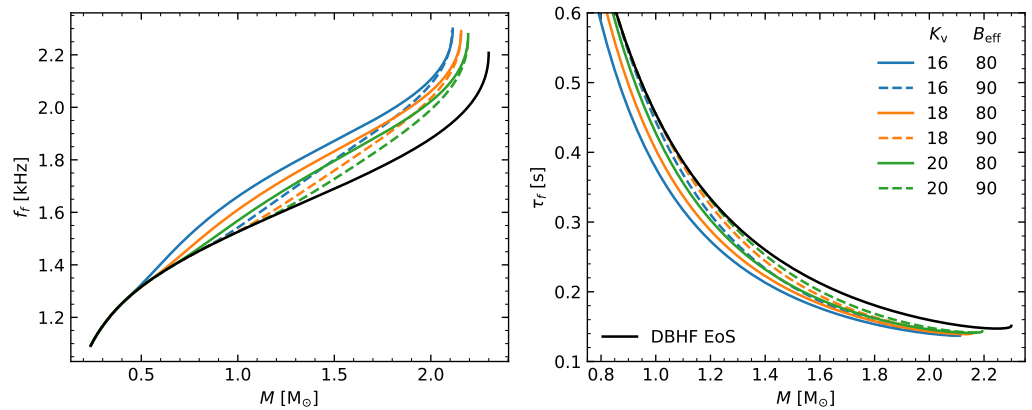


**Figure 6.** Frequency (left panel) and damping time (right panel) of  $f$ -mode as a function of the stellar mass of hybrid stars with different quark matter EoSs. The blue, orange, and green lines are for  $K_v = 16, 18,$  and  $20 \text{ GeV}^{-2}$ , respectively. The solid and dashed lines are for  $B_{\text{eff}} = 80$  and  $90 \text{ MeV fm}^{-3}$ , respectively. The results for the neutron star in the DBHF EoS are shown for comparison with solid black line.

It is necessary to test our results with the well-established universal relations mentioned in the previous works [40,46,47]. Obviously, they enable us to constrain the predicted features of  $f$ -mode oscillations using the existing data of the pulsar observations and terrestrial laboratory constraints on the EoS parameters. In general, a complex eigen-frequency  $\omega = \omega_r - i\omega_i$  is used to characterize the quasi-normal modes [41,74–76], where  $\omega_r$  is the frequency of  $f$ -mode  $2\pi f_f$  and  $\omega_i$  is the damping rate  $1/\tau_f$ . The universal relations between a star mass scaled by frequency  $M\omega$  and macrostructure quantities, such as compactness [48] and tidal deformability [49,50,77,78], are almost independent of the EoSs, and the power law expansion can be used to describe the complex frequency of  $f$ -mode [50,79].

For the results between mass scaled frequency  $M\omega$  and compactness  $C$ , we use the following expression for fitting:

$$M\omega_r = \sum_{j=0}^4 a_j C^j, \tag{12}$$

$$M\omega_i = \sum_{j=0}^7 a_j C^j. \tag{13}$$

For the results between mass scaled frequency  $M\omega$  and dimensionless tidal deformability  $\Lambda$ , we use the following expression for fitting:

$$M\omega = \sum_{j=0}^4 a_j (\ln \Lambda)^j. \tag{14}$$

The coefficients  $a_j$  of Equations (12)–(14) are complex numbers corresponding to  $\omega_r$  and  $\omega_i$ . Compactness and complex frequency are presented in geometrized units with  $c = G = 1$ . We check that adding an additional term of the power law does not offer much improvement in the accuracy for our fits, but by altering coefficients, we are able to improve the fit for high compactness. Thus, we use fourth-order (seventh-order) polynomials to fit the relations between the the real part (imaginary part) of the eigen-frequency of  $f$ -mode and compactness and fourth-order polynomials to fit the relations between the complex frequency and dimensionless tidal deformability, respectively. The coefficients  $a_j$  and the  $R^2$  statistic for the best fit are shown in Table 1. These universal relations have higher accuracy (with a standard statistical correlation coefficient large than 0.9994) in a wide range of compactness ( $0.019 < C < 0.296$ ).

**Table 1.** Coefficients and the  $R^2$  statistic for the best fit of Equations (12)–(14).

	$a_0$	$a_1$	$a_2$	$a_3$	$a_4$	$a_5$	$a_6$	$a_7$	$R^2$
$M\omega_r - C$	$8.162 \times 10^{-4}$	$2.760 \times 10^{-1}$	1.116	$2.318 \times 10^{-1}$	-3.641	...	...	...	0.9994
$M\omega_i - C$	$-2.514 \times 10^{-8}$	$-9.301 \times 10^{-7}$	$3.172 \times 10^{-4}$	$-9.566 \times 10^{-4}$	$8.581 \times 10^{-2}$	$-4.117 \times 10^{-1}$	$6.562 \times 10^{-1}$	$-4.655 \times 10^{-1}$	0.9997
$M\omega_r - \Lambda$	$1.827 \times 10^{-1}$	$-7.219 \times 10^{-3}$	$-4.172 \times 10^{-3}$	$5.311 \times 10^{-4}$	$-1.957 \times 10^{-5}$	...	...	...	0.999995
$M\omega_i - \Lambda$	$1.963 \times 10^{-5}$	$5.749 \times 10^{-5}$	$-1.850 \times 10^{-5}$	$1.972 \times 10^{-6}$	$-7.147 \times 10^{-8}$	...	...	...	0.999976

The fitting curves of the scaled complex frequency of  $f$ -mode versus compactness are shown in the top panels of Figure 7. For comparison, we also plot some previous fitting results in Tsui and Leung [48], Zhao and Lattimer [50]. In this figure, we consider different masses with the constraints of EoS parameters when the mixed phase appears in the hybrid stars. The bottom panels in Figure 7 show the relative errors of our fit to the computed results of all EoS parameters of hybrid star in our work. Moderate relative errors (12%) are limited to small compactness  $C < 0.03$  with the existence of a mixed phase, and the maximum relative error in the remaining compactness regions is less than 7%, especially in  $C > 0.25$ . Fits for the real part of  $\omega$  where the relative errors are smaller than 4.8% are somewhat more accurate than those for the imaginary part. It is suggested that this universal relation is still suitable for the hybrid star in the vBag model. The results of low-mass hybrid stars are included in our fits, and our results characterize the behavior of a wide range of compactness well.

The fitting results of the complex frequency of  $f$ -mode versus dimensionless tidal deformability  $\Lambda$  are shown in Figure 8. For comparison, we also plot some previous fitting results in Chan et al. [49], Zhao and Lattimer [50]. The relative errors of the real part of the scaled frequency versus  $\Lambda$  are much smaller than 0.3% ( $<0.3\%$ ), and the relative errors of the scaled damping rate versus  $\Lambda$  are smaller than 1.3% ( $<1.3\%$ ). All results for the real and imaginary parts' scaled frequencies of hybrid stars are almost on a curve, with no significant dispersion. Moreover, the fitted curves also almost overlap with the results of previous works.

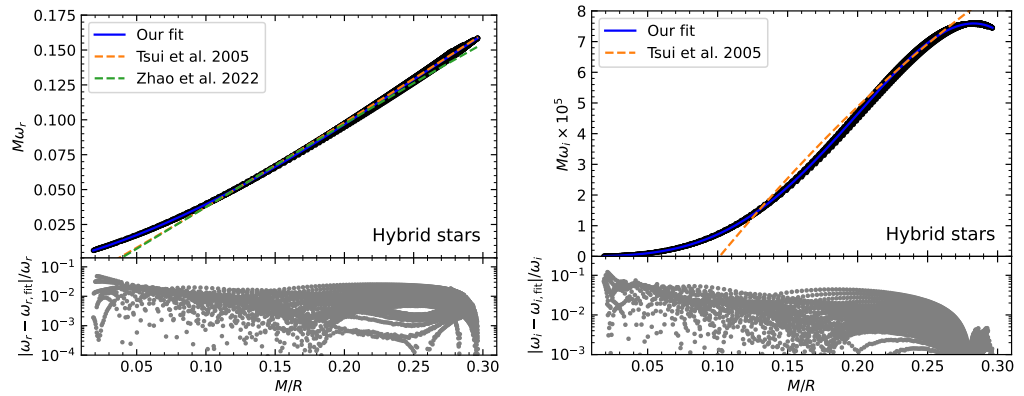


**Figure 7.** Mass scaled complex frequency of  $f$ -mode as a function of compactness for hybrid stars in the vBag model that satisfy multi-messenger observational constraints. The (left,right) panel shows the real (imaginary) part of the mass scaled frequency. **Top panel:** The black dots are the calculation results of hybrid stars. The blue lines are the fitting results of our work. The orange dashed lines are for the fitting results of Tsui and Leung [48], and the green dashed line is for the fitting results of Zhao and Lattimer [50]. **Bottom panel:** The relative errors of our fit for the computed results for all parameters in our work.

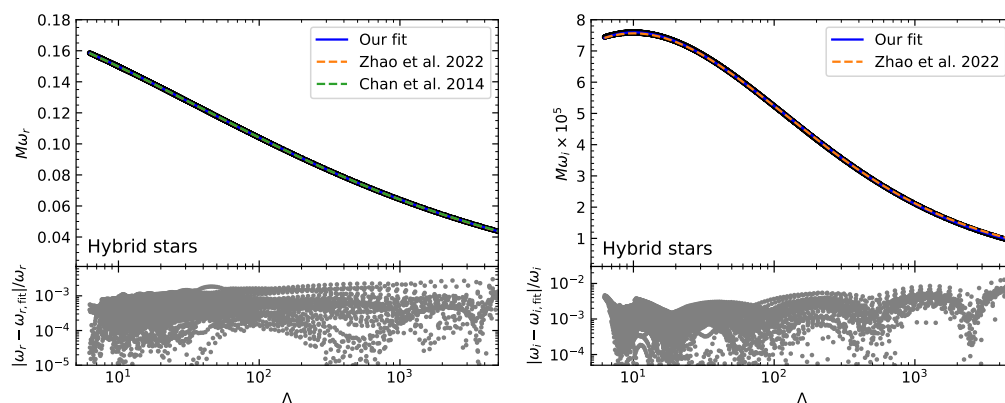


**Figure 8.** Mass scaled complex frequency of  $f$ -mode as a function of tidal deformability for hybrid stars in the  $\nu$ Bag model that satisfy multi-messenger observational constraints. The (left, right) panel shows the real (imaginary) part of the mass scaled frequency. **Top** panel: The black dots are the calculation results of hybrid stars. The blue line is our fitting result. The orange dashed line is the result of Chan et al. [49], and the green dashed line is for Zhao and Lattimer [50]. **Bottom** panel: The relative errors of our fit from the computed results for all parameters in our work.

### 5. Conclusions

The tidal deformability, masses, and radii of pulsars provide a powerful way to constrain the EoSs of dense matter at high densities. Combining these observational results, we constrain the parameters of the  $\nu$ Bag model within the framework of strange stars and hybrid stars (under Gibbs construction). Based on the limitations of the EoS of quark matter, we study the correlations among the  $f$ -mode frequency and, its damping time and the compactness and tidal deformability of hybrid stars.

We find that the lower values of  $K_V$  and  $B_{\text{eff}}$  result in a decrease in the phase transition density from hadronic phase to mixed phase. In addition, the phase transitions occur inside hybrid stars at very low density (around nuclear saturation density), which allows mixed phases to appear in the low-mass stars (around 0.2 solar mass). For massive stars, the mixed phase may occupy a large region in which its radius and mass ratio surpasses 0.8. Furthermore, the  $\nu$ Bag model cannot simultaneously satisfy the current multi-messenger observation constraints within the framework of strange stars.

Our results for the  $\ell = 2$   $f$ -mode oscillation frequency and damping time reveal that the appearance of the mixed phase inside the hybrid star causes a rise in the oscillation frequency and a decrease in the damping time, respectively. The softer EoS makes this variation more apparent due to the more significant reduction in radius. The test of two common universal relations of hybrid stars reveals a high correlation between  $f$ -mode complex frequency and compactness/dimensionless tidal deformability, which is well-fitted by a power law expansion. The hybrid stars in the  $\nu$ Bag model do not contradict this universality, but our results expand the fitting compactness range. Thus, gravitational waves excited by  $f$ -mode oscillations of compact stars may provide valuable and complementary information on the features of compact stars and the underlying nature of quark matter.

**Author Contributions:** Software, H.-Y.Z. and W.W.; writing—review and editing, X.Z. and W.W.; data curation, H.-Y.Z. and W.W.; writing—original draft preparation, H.-Y.Z.; methodology, X.Z. and W.W.; funding acquisition, X.Z. and W.W. All authors have read and agreed to the published version of the manuscript.

**Funding:** This research was funded by the CAS “Light of West China” Program No. 2019-XBQNXZ-B-016, the National Natural Science Foundation of China (Grant Nos. 12033001, 12288102, 12273028), the Opening Foundation of Xinjiang Key Laboratory (No. 2021D04016), and the Major Science and Technology Program of Xinjiang Uygur Autonomous Region (No. 2022A03013-1).

**Data Availability Statement:** Observational data used in this paper are quoted from the cited works. Additional data generated from computations can be made available upon reasonable request.

**Acknowledgments:** We would like to thank the anonymous referee for their helpful suggestions that led to significant improvements in our study. X.Z. would like to thank Qing-min Li for her fruitful suggestions.

**Conflicts of Interest:** The authors declare no conflicts of interest.

## References

1. Blaschke, D.; Chamel, N. Phases of Dense Matter in Compact Stars. In *The Physics and Astrophysics of Neutron Stars*; Rezzolla, L., Pizzochero, P., Jones, D.I., Rea, N., Vidaña, I., Eds.; Astrophysics and Space Science Library; Springer: Cham, Switzerland, 2018; Volume 457, p. 337. [[CrossRef](#)]
2. Endo, T. Appearance of a quark matter phase in hybrid stars. *J. Phys. Conf. Ser.* **2014**, *509*, 012075. [[CrossRef](#)]
3. Buballa, M. Phase diagram of quark matter under compact star conditions. In *Quark Confinement and the Hadron Spectrum VII*; Ribeiro, J.E.F.T., Brambilla, N., Vairo, A., Maung, K., Prospero, G.M., Eds.; American Institute of Physics Conference Series; American Institute of Physics: Melville, NY, USA, 2007; Volume 892, pp. 476–478. [[CrossRef](#)]
4. Abbott, B.P.; Abbott, R.; Abbott, T.D.; Acernese, F.; Ackley, K.; Adams, C.; Adams, T.; Addesso, P.; Adhikari, R.X.; Adya, V.B.; et al. GW170817: Observation of Gravitational Waves from a Binary Neutron Star Inspiral. *Phys. Rev. Lett.* **2017**, *119*, 161101. [[CrossRef](#)] [[PubMed](#)]
5. Radice, D.; Perego, A.; Zappa, F.; Bernuzzi, S. GW170817: Joint Constraint on the Neutron Star Equation of State from Multimessenger Observations. *Astrophys. J. Lett.* **2018**, *852*, L29. [[CrossRef](#)]
6. Chatziioannou, K.; Haster, C.J.; Zimmerman, A. Measuring the neutron star tidal deformability with equation-of-state-independent relations and gravitational waves. *Phys. Rev. D* **2018**, *97*, 104036. [[CrossRef](#)]
7. Malik, T.; Alam, N.; Fortin, M.; Providência, C.; Agrawal, B.K.; Jha, T.K.; Kumar, B.; Patra, S.K. GW170817: Constraining the nuclear matter equation of state from the neutron star tidal deformability. *Phys. Rev. C* **2018**, *98*, 035804. [[CrossRef](#)]
8. Tews, I.; Margueron, J.; Reddy, S. Critical examination of constraints on the equation of state of dense matter obtained from GW170817. *Phys. Rev. C* **2018**, *98*, 045804. [[CrossRef](#)]
9. Zhu, Z.Y.; Zhou, E.P.; Li, A. Neutron Star Equation of State from the Quark Level in Light of GW170817. *Astrophys. J.* **2018**, *862*, 98. [[CrossRef](#)]
10. Paschalidis, V.; Yagi, K.; Alvarez-Castillo, D.; Blaschke, D.B.; Sedrakian, A. Implications from GW170817 and I-Love-Q relations for relativistic hybrid stars. *Phys. Rev. D* **2018**, *97*, 084038. [[CrossRef](#)]
11. Nandi, R.; Char, P. Hybrid Stars in the Light of GW170817. *Astrophys. J.* **2018**, *857*, 12. [[CrossRef](#)]
12. Christian, J.E.; Zacchi, A.; Schaffner-Bielich, J. Signals in the tidal deformability for phase transitions in compact stars with constraints from GW170817. *Phys. Rev. D* **2019**, *99*, 023009. [[CrossRef](#)]
13. Demorest, P.B.; Pennucci, T.; Ransom, S.M.; Roberts, M.S.E.; Hessels, J.W.T. A two-solar-mass neutron star measured using Shapiro delay. *Nature* **2010**, *467*, 1081–1083. [[CrossRef](#)] [[PubMed](#)]
14. Antoniadis, J.; Freire, P.C.C.; Wex, N.; Tauris, T.M.; Lynch, R.S.; van Kerkwijk, M.H.; Kramer, M.; Bassa, C.; Dhillon, V.S.; Driebe, T.; et al. A Massive Pulsar in a Compact Relativistic Binary. *Science* **2013**, *340*, 448. [[CrossRef](#)] [[PubMed](#)]
15. Cromartie, H.T.; Fonseca, E.; Ransom, S.M.; Demorest, P.B.; Arzoumanian, Z.; Blumer, H.; Brook, P.R.; DeCesar, M.E.; Dolch, T.; Ellis, J.A.; et al. Relativistic Shapiro delay measurements of an extremely massive millisecond pulsar. *Nat. Astron.* **2020**, *4*, 72–76. [[CrossRef](#)]
16. Fonseca, E.; Cromartie, H.T.; Pennucci, T.T.; Ray, P.S.; Kirichenko, A.Y.; Ransom, S.M.; Demorest, P.B.; Stairs, I.H.; Arzoumanian, Z.; Guillemot, L.; et al. Refined Mass and Geometric Measurements of the High-mass PSR J0740+6620. *Astrophys. J. Lett.* **2021**, *915*, L12. [[CrossRef](#)]
17. Riley, T.E.; Watts, A.L.; Bogdanov, S.; Ray, P.S.; Ludlam, R.M.; Guillot, S.; Arzoumanian, Z.; Baker, C.L.; Bilous, A.V.; Chakrabarty, D.; et al. A NICER View of PSR J0030+0451: Millisecond Pulsar Parameter Estimation. *Astrophys. J. Lett.* **2019**, *887*, L21. [[CrossRef](#)]
18. Riley, T.E.; Watts, A.L.; Ray, P.S.; Bogdanov, S.; Guillot, S.; Morsink, S.M.; Bilous, A.V.; Arzoumanian, Z.; Choudhury, D.; Deneva, J.S.; et al. A NICER View of the Massive Pulsar PSR J0740+6620 Informed by Radio Timing and XMM-Newton Spectroscopy. *Astrophys. J. Lett.* **2021**, *918*, L27. [[CrossRef](#)]
19. Miller, M.C.; Lamb, F.K.; Dittmann, A.J.; Bogdanov, S.; Arzoumanian, Z.; Gendreau, K.C.; Guillot, S.; Harding, A.K.; Ho, W.C.G.; Lattimer, J.M.; et al. PSR J0030+0451 Mass and Radius from NICER Data and Implications for the Properties of Neutron Star Matter. *Astrophys. J. Lett.* **2019**, *887*, L24. [[CrossRef](#)]
20. Miller, M.C.; Lamb, F.K.; Dittmann, A.J.; Bogdanov, S.; Arzoumanian, Z.; Gendreau, K.C.; Guillot, S.; Ho, W.C.G.; Lattimer, J.M.; Loewenstein, M.; et al. The Radius of PSR J0740+6620 from NICER and XMM-Newton Data. *Astrophys. J. Lett.* **2021**, *918*, L28. [[CrossRef](#)]
21. Cottam, J.; Paerels, F.; Mendez, M. Gravitationally redshifted absorption lines in the X-ray burst spectra of a neutron star. *Nature* **2002**, *420*, 51–54. [[CrossRef](#)]
22. Özel, F. Soft equations of state for neutron-star matter ruled out by EXO 0748-676. *Nature* **2006**, *441*, 1115–1117. [[CrossRef](#)]

23. Chodos, A.; Jaffe, R.L.; Johnson, K.; Thorn, C.B.; Weisskopf, V.F. New extended model of hadrons. *Phys. Rev. D* **1974**, *9*, 3471–3495. [[CrossRef](#)]
24. Rüter, S.B.; Rischke, D.H. Effect of color superconductivity on the mass and radius of a quark star. *Phys. Rev. D* **2004**, *69*, 045011. [[CrossRef](#)]
25. Horvath, J.E.; Lugones, G. Self-bound CFL stars in binary systems: Are they “hidden” among the black hole candidates? *Astron. Astrophys.* **2004**, *422*, L1–L4. :20040180. [[CrossRef](#)]
26. Farhi, E.; Jaffe, R.L. Strange matter. *Phys. Rev. D* **1984**, *30*, 2379–2390. [[CrossRef](#)]
27. Fraga, E.S.; Pisarski, R.D.; Schaffner-Bielich, J. Small, dense quark stars from perturbative QCD. *Phys. Rev. D* **2001**, *63*, 121702. [[CrossRef](#)]
28. Klähn, T.; Fischer, T. Vector Interaction Enhanced Bag Model for Astrophysical Applications. *Astrophys. J.* **2015**, *810*, 134. [[CrossRef](#)]
29. Gomes, R.O.; Char, P.; Schramm, S. Constraining Strangeness in Dense Matter with GW170817. *Astrophys. J.* **2019**, *877*, 139. [[CrossRef](#)]
30. Nambu, Y.; Jona-Lasinio, G. Dynamical Model of Elementary Particles Based on an Analogy with Superconductivity. I. *Phys. Rev.* **1961**, *122*, 345–358. [[CrossRef](#)]
31. Nambu, Y.; Jona-Lasinio, G. Dynamical Model of Elementary Particles Based on an Analogy with Superconductivity. II. *Phys. Rev.* **1961**, *124*, 246–254. [[CrossRef](#)]
32. Alford, M.; Blaschke, D.; Drago, A.; Klähn, T.; Pagliara, G.; Schaffner-Bielich, J. Astrophysics: Quark matter in compact stars? *Nature* **2007**, *445*, 7–8. [[CrossRef](#)]
33. Rodrigues, H.; Duarte, S.B.; Oliveira, J.C.T. EXO 0748-676 as a Quark Star. *Int. J. Mod. Phys. D* **2010**, *19*, 1447–1454. [[CrossRef](#)]
34. Sotani, H.; Yasutake, N.; Maruyama, T.; Tatsumi, T. Signatures of hadron-quark mixed phase in gravitational waves. *Phys. Rev. D* **2011**, *83*, 024014. [[CrossRef](#)]
35. Sotani, H.; Maruyama, T.; Tatsumi, T. Shear oscillations in the hadron-quark mixed phase. *Nucl. Phys. A* **2013**, *906*, 37–49. [[CrossRef](#)]
36. Brillante, A.; Mishustin, I.N. Radial oscillations of neutral and charged hybrid stars. *EPL (Europhys. Lett.)* **2014**, *105*, 39001. [[CrossRef](#)]
37. Vásquez Flores, C.; Lugones, G. Non-radial fluid oscillation modes of color superconducting self-bound stars. *Astron. Nachrichten* **2014**, *335*, 769. [[CrossRef](#)]
38. Wei, W.; Irving, B.; Salinas, M.; Klähn, T.; Jaikumar, P. Camouflage of the Phase Transition to Quark Matter in Neutron Stars. *Astrophys. J.* **2019**, *887*, 151. [[CrossRef](#)]
39. Wei, W.; Salinas, M.; Klähn, T.; Jaikumar, P.; Barry, M. Lifting the Veil on Quark Matter in Compact Stars with Core g-mode Oscillations. *Astrophys. J.* **2020**, *904*, 187. [[CrossRef](#)]
40. Andersson, N.; Kokkotas, K.D. Towards gravitational wave asteroseismology. *Mon. Not. R. Astron. Soc.* **1998**, *299*, 1059–1068. [[CrossRef](#)]
41. Kokkotas, K.D.; Schmidt, B.G. Quasi-Normal Modes of Stars and Black Holes. *Living Rev. Relativ.* **1999**, *2*, 2. [[CrossRef](#)]
42. Kokkotas, K.D.; Apostolatos, T.A.; Andersson, N. The inverse problem for pulsating neutron stars: A ‘fingerprint analysis’ for the supranuclear equation of state. *Mon. Not. R. Astron. Soc.* **2001**, *320*, 307–315. [[CrossRef](#)]
43. Punturo, M.; Abernathy, M.; Acernese, F.; Allen, B.; Andersson, N.; Arun, K.; Barone, F.; Barr, B.; Barsuglia, M.; Beker, M.; et al. The Einstein Telescope: A third-generation gravitational wave observatory. *Class. Quantum Gravity* **2010**, *27*, 194002. [[CrossRef](#)]
44. Abbott, B.P.; Abbott, R.; Abbott, T.D.; Abernathy, M.R.; Ackley, K.; Adams, C.; Addesso, P.; Adhikari, R.X.; Adya, V.B.; Affeldt, C.; et al. Exploring the sensitivity of next generation gravitational wave detectors. *Class. Quantum Gravity* **2017**, *34*, 044001. [[CrossRef](#)]
45. Abbott, B.P.; Abbott, R.; Abbott, T.D.; Acernese, F.; Ackley, K.; Adams, C.; Adams, T.; Addesso, P.; Adhikari, R.X.; Adya, V.B.; et al. Properties of the Binary Neutron Star Merger GW170817. *Phys. Rev. X* **2019**, *9*, 011001. [[CrossRef](#)]
46. Benhar, O.; Berti, E.; Ferrari, V. The imprint of the equation of state on the axial w-modes of oscillating neutron stars. *Mon. Not. R. Astron. Soc.* **1999**, *310*, 797–803. [[CrossRef](#)]
47. Benhar, O.; Ferrari, V.; Gualtieri, L. Gravitational wave asteroseismology reexamined. *Phys. Rev. D* **2004**, *70*, 124015. [[CrossRef](#)]
48. Tsui, L.K.; Leung, P.T. Universality in quasi-normal modes of neutron stars. *Mon. Not. R. Astron. Soc.* **2005**, *357*, 1029–1037. [[CrossRef](#)]
49. Chan, T.K.; Sham, Y.H.; Leung, P.T.; Lin, L.M. Multipolar universal relations between f-mode frequency and tidal deformability of compact stars. *Phys. Rev. D* **2014**, *90*, 124023. [[CrossRef](#)]
50. Zhao, T.; Lattimer, J.M. Universal relations for neutron star f-mode and g-mode oscillations. *Phys. Rev. D* **2022**, *106*, 123002. [[CrossRef](#)]
51. Aziz, A.; Ray, S.; Rahaman, F.; Khlopov, M.; Guha, B.K. Constraining values of bag constant for strange star candidates. *Int. J. Mod. Phys. D* **2019**, *28*, 1941006. [[CrossRef](#)]
52. Das, S.; Ray, S.; Khlopov, M.; Nandi, K.K.; Parida, B.K. Anisotropic compact stars: Constraining model parameters to account for physical features of tidal Love numbers. *Ann. Phys.* **2021**, *433*, 168597. [[CrossRef](#)]
53. Lattimer, J.M.; Prakash, M. Neutron Star Structure and the Equation of State. *Astrophys. J.* **2001**, *550*, 426–442. [[CrossRef](#)]

54. Glendenning, N.K. First-order phase transitions with more than one conserved charge: Consequences for neutron stars. *Phys. Rev. D* **1992**, *46*, 1274–1287. [[CrossRef](#)] [[PubMed](#)]
55. Baym, G.; Bethe, H.A.; Pethick, C.J. Neutron star matter. *Nucl. Phys. A* **1971**, *175*, 225–271. [[CrossRef](#)]
56. Baym, G.; Pethick, C.; Sutherland, P. The Ground State of Matter at High Densities: Equation of State and Stellar Models. *Astrophys. J.* **1971**, *170*, 299. [[CrossRef](#)]
57. Fuchs, C. The Relativistic Dirac-Brueckner Approach to Nuclear Matter. In *Extended Density Functionals in Nuclear Structure Physics*; Lalazissis, G.A., Ring, P., Vretenar, D., Eds.; Springer: Berlin/Heidelberg, Germany, 2004; Volume 641, pp. 119–146. [[CrossRef](#)]
58. van Dalen, E.N.E.; Fuchs, C.; Faessler, A. The relativistic Dirac-Brueckner approach to asymmetric nuclear matter. *Nucl. Phys. A* **2004**, *744*, 227–248. [[CrossRef](#)]
59. Klähn, T.; Blaschke, D.; Typel, S.; van Dalen, E.N.E.; Faessler, A.; Fuchs, C.; Gaitanos, T.; Grigorian, H.; Ho, A.; Kolomeitsev, E.E.; et al. Constraints on the high-density nuclear equation of state from the phenomenology of compact stars and heavy-ion collisions. *Phys. Rev. C* **2006**, *74*, 035802. [[CrossRef](#)]
60. Glendenning, N.K. *Compact Stars. Nuclear Physics, Particle Physics, and General Relativity*; Springer: New York, NY, USA, 1997.
61. Tolman, R.C. Static Solutions of Einstein's Field Equations for Spheres of Fluid. *Phys. Rev.* **1939**, *55*, 364–373. [[CrossRef](#)]
62. Oppenheimer, J.R.; Volkoff, G.M. On Massive Neutron Cores. *Phys. Rev.* **1939**, *55*, 374–381. [[CrossRef](#)]
63. Flanagan, É.É.; Hinderer, T. Constraining neutron-star tidal Love numbers with gravitational-wave detectors. *Phys. Rev. D* **2008**, *77*, 021502. [[CrossRef](#)]
64. Hinderer, T. Tidal Love Numbers of Neutron Stars. *Astrophys. J.* **2008**, *677*, 1216–1220. [[CrossRef](#)]
65. Damour, T.; Nagar, A. Relativistic tidal properties of neutron stars. *Phys. Rev. D* **2009**, *80*, 084035. [[CrossRef](#)]
66. Arzoumanian, Z.; Brazier, A.; Burke-Spolaor, S.; Chamberlin, S.; Chatterjee, S.; Christy, B.; Cordes, J.M.; Cornish, N.J.; Crawford, F.; Thankful Cromartie, H.; et al. The NANOGrav 11-year Data Set: High-precision Timing of 45 Millisecond Pulsars. *Astrophys. J. Suppl. Ser.* **2018**, *235*, 37. <https://doi.org/10.3847/1538-4365/aab5b0>. [[CrossRef](#)]
67. Romani, R.W.; Kandel, D.; Filippenko, A.V.; Brink, T.G.; Zheng, W. PSR J1810+1744: Companion Darkening and a Precise High Neutron Star Mass. *Astrophys. J. Lett.* **2021**, *908*, L46. [[CrossRef](#)]
68. Romani, R.W.; Kandel, D.; Filippenko, A.V.; Brink, T.G.; Zheng, W. PSR J0952-0607: The Fastest and Heaviest Known Galactic Neutron Star. *Astrophys. J. Lett.* **2022**, *934*, L17. [[CrossRef](#)]
69. Abbott, B.P.; Abbott, R.; Abbott, T.D.; Acernese, F.; Ackley, K.; Adams, C.; Adams, T.; Addesso, P.; Adhikari, R.X.; Adya, V.B.; et al. GW170817: Measurements of Neutron Star Radii and Equation of State. *Phys. Rev. Lett.* **2018**, *121*, 161101. [[CrossRef](#)] [[PubMed](#)]
70. Witten, E. Cosmic separation of phases. *Phys. Rev. D* **1984**, *30*, 272–285. [[CrossRef](#)]
71. Weissenborn, S.; Sagert, I.; Pagliara, G.; Hempel, M.; Schaffner-Bielich, J. Quark Matter in Massive Compact Stars. *Astrophys. J. Lett.* **2011**, *740*, L14. [[CrossRef](#)]
72. Lindblom, L.; Detweiler, S.L. The quadrupole oscillations of neutron stars. *Astrophys. J.* **1983**, *53*, 73–92. [[CrossRef](#)]
73. Detweiler, S.; Lindblom, L. On the nonradial pulsations of general relativistic stellar models. *Astrophys. J.* **1985**, *292*, 12–15. [[CrossRef](#)]
74. Press, W.H. Long Wave Trains of Gravitational Waves from a Vibrating Black Hole. *Astrophys. J. Lett.* **1971**, *170*, L105. [[CrossRef](#)]
75. Leaver, E.W. Spectral decomposition of the perturbation response of the Schwarzschild geometry. *Phys. Rev. D* **1986**, *34*, 384–408. [[CrossRef](#)] [[PubMed](#)]
76. Ching, E.S.C.; Leung, P.T.; Suen, W.M.; Young, K. Wave propagation in gravitational systems: Completeness of quasinormal modes. *Phys. Rev. D* **1996**, *54*, 3778–3791. [[CrossRef](#)] [[PubMed](#)]
77. Chirenti, C.; de Souza, G.H.; Kastaun, W. Fundamental oscillation modes of neutron stars: Validity of universal relations. *Phys. Rev. D* **2015**, *91*, 044034. [[CrossRef](#)]
78. Lioutas, G.; Bauswein, A.; Stergioulas, N. Frequency deviations in universal relations of isolated neutron stars and postmerger remnants. *Phys. Rev. D* **2021**, *104*, 043011. [[CrossRef](#)]
79. Lioutas, G.; Stergioulas, N. Universal and approximate relations for the gravitational-wave damping timescale of f-modes in neutron stars. *Gen. Relativ. Gravit.* **2018**, *50*, 12. [[CrossRef](#)]

**Disclaimer/Publisher's Note:** The statements, opinions and data contained in all publications are solely those of the individual author(s) and contributor(s) and not of MDPI and/or the editor(s). MDPI and/or the editor(s) disclaim responsibility for any injury to people or property resulting from any ideas, methods, instructions or products referred to in the content.